Ionospheric TEC and Plasma Parameters Anomalies Associated with the 14 July 2019 Mw7.2 Laiwui Earthquake Detected by the GPS and CSES

Preprint · February 2021

DOI: 10.21203/rs.3.rs-223597/v1

6 authors, including:

Yuanzheng Wen
Chengdu University of Technology
4 PUBLICATIONS **2** CITATIONS
SEE PROFILE

Zeren Zhima
National Institute of Natural Hazards MEMC
59 PUBLICATIONS **579** CITATIONS
SEE PROFILE

Xuhui Shen
China Earthquake Administration
121 PUBLICATIONS **925** CITATIONS
SEE PROFILE

Ionospheric TEC and plasma anomalies associated with the 14 July 2019 M_w7.2 Laiwui earthquake detected by the GPS and CSES

Yuanzheng Wen[1,2], Dan Tao[1,2], Guangxue Wang[1,2], Jiayi Zong[1,2], Jinbin Cao[3], Roberto Battiston[4], Zhima Zeren[5], Xuhui Shen[5]

[1] Key Laboratory of Earth Exploration and Information Techniques of Ministry of Education, Chengdu University of Technology, Chengdu, China.

[2] College of Geophysics, Chengdu University of Technology, Chengdu, China.

[3] School of Space and Environment, Beihang University, Beijing, China.

[4] Dipartimento di Fisica, Università di Trento, Trento, Italy.

[5] National Institute of Natural Hazards, Ministry of Emergency Management of China, Beijing, China.

Correspondence to: Dan Tao (dan.tao@cdut.edu.cn)

Author #1: Yuanzheng Wen, Chengdu University of Technology, Chengdu, China, wenyuanzheng@stu.cdut.edu.cn

Author #2: Dan Tao, Chengdu University of Technology, Chengdu, China, dan.tao@cdut.edu.cn (Corresponding Author)

Author #3: Guangxue Wang, Chengdu University of Technology, Chengdu, China, wangguangxue@stu.cdut.edu.cn

Author #4: Jiayi Zong, Chengdu University of Technology, Chengdu, China

zongjiayi@stu.cdut.edu.cn

Author #5: Jinbin Cao, School of Space and Environment, Beihang University, Beijing, China, jbcao@buaa.edu.cn

Author #6: Roberto Battiston, Dipartimento di Fisica, Università di Trento, Trento, Italy, roberto.battiston@unitn.it

Author #7: Zhima Zeren, National Institute of Natural Hazards, Ministry of Emergency Management of China, Beijing, China, zrzm@seis.ac.cn

Author #8: Xuhui Shen, National Institute of Natural Hazards, Ministry of Emergency Management of China, Beijing, China, shenxh@seis.ac.cn

Abstract

In this study, with cross-valid analysis of total electron content (TEC) data of the global ionospheric map (GIM) from GPS and plasma parameters data recorded by China Seismo-Electromagnetic Satellite (CSES), signatures of seismic-ionospheric perturbations related to the 14 July 2019 M_w7.2 Laiwui earthquake were detected. After distinguishing the solar and geomagnetic activities, three positive temporal anomalies were found around the epicenter 1 day, 3 days and 8 days before the earthquake (14 July 2019) along with a negative anomaly 6 days after the earthquake, which also agrees well with the TEC spatial variations in latitude-longitude-time (LLT) maps. To further confirm the anomalies, the ionospheric plasma parameters (electron, O^+ and He^+ densities) recorded by the Langmuir probe (LAP) and Plasma Analyzer Package (PAP) onboard CSES were analyzed by using the moving mean method (MMM), which also presented remarkable enhancements along the orbits around the epicenter on day 2, day 4 and day 7 before the earthquake. To make the investigations more convincing, the disturbed orbits were compared with their corresponding four nearest revisiting orbits, whose results indeed indicate the existence of plasma parameters anomalies associated with the Laiwui

47 earthquake. All these results illustrated that the GPS and CSES observed unusual
48 ionospheric perturbations are highly associated with the M_w7.2 Laiwui earthquake,
49 which also strongly indicates the existence of pre-seismic ionospheric anomalies over the
50 earthquake region.

51 **Keywords**

52 Seismic-ionospheric perturbations; CSES satellite; Ionosphere; Earthquake

53 ## 1. Introduction

54 Electromagnetic phenomena possibly associated with natural disasters (earthquake,
55 tsunami and volcanic activities) have been extensively investigated in recent years, and
56 seismic related anomalies are the most important ones. Although the physical mechanism
57 about the seismic ionospheric anomalies is still unclear, a significant number of
58 observational studies suggest that there is indeed a connection between the two
59 phenomena. In general, the seismic ionospheric disturbance mainly includes the
60 "earthquake precursor" effect of ionospheric TEC and plasma parameters.

61 There are currently two major types of methods for the measurement of seismic
62 associated ionospheric anomalies: the ground-based stations and space-based satellites.
63 The total electron content (TEC) derived from measurements of local ground-based GPS
64 receivers was first employed by Liu et al. (2001) to study ionospheric electron density
65 variations during the 1999 M_w7.6 ChiChi earthquake and he found that the GPS TEC

around the epicenter dramatically decrease in the afternoon period a day, 3 days, and 4 days before the earthquake. After that, Liu et al. (2004) further confirmed this pre-seismic precursor by conducting a statistical investigation of global ionospheric map (GIM) based on 20 $M_W \geq 6.0$ earthquakes during a period of 4 years from 1999-2002 in Taiwan., which demonstrates that the GPS TECs significantly decrease in the afternoon/evening period within 5 days prior to 16 of the 20 earthquakes. Following those, a number of related investigations were conducted by applying the GIM to study TEC anomalies before strong earthquakes with more reliable statistical methods. For instance, clear precursory positive anomalies of ionospheric total electron content (TEC) were found around the focal region prior to the 2011 Mw9.0 Tohoku - Oki earthquake (Liu et al.,2011; Heki et al.,2011). While, Kon et al. (2011) analyzed $M_w \geq 6.0$ earthquakes which occurred in Japan from 1998 to 2010 by the superposed epoch analysis (SEA) method, and the positive TEC anomalies 1–5 days ahead were detected within 1000 km from the epicenters. It is also found that the TEC over the epicenter significantly enhances on a day before the 12 January 2010 M7 Haiti earthquake. The TECs of the two Mid-latitude dense strips on 35◦ N/60◦ S and those of Seismic-ionospheric anomalies in ionospheric TEC and plasma density of the epicenter/conjugate point reach their maximum values on a day before the earthquake, while the northern crest of equatorial ionization anomaly (EIA) moves poleward (Liu et al., 2011).

In most cases, however, the measurement of ground-based stations can be rather limited. Since there is a lack of extensive ground experiments to monitor geophysical and

87 geochemical parameters in most areas. Thus, space-based satellite experiment with the
88 vast coverage of the seismic areas of Earth can be regarded as a more effective way for
89 measurements of seismic-ionospheric effects (Akhoondzadeh et al., 2010). The
90 DEMETER (Detection of ElectroMagnetic Emissions Transmitted from Earthquake
91 Regions) satellite data have already been applied to many studies. With the DEMETER
92 data, a number of perturbations have been found before some strong earthquakes.
93 Anomalies in the O^+ density, ion temperature, electric field, and ELF/VLF/ULF
94 emissions around the epicenter region detected by DEMETER were considered to be
95 highly associated with the 12 May 2008 M8.0 Wenchuan earthquake (Zhang et al.2009,
96 2012). A statistical investigation by Akhoondzadeh et al. (2010) made the simultaneous
97 observations of positive and negative anomalies in both DEMETER and GPS data during
98 1-5 days before all studied earthquakes under weak and quiet geomagnetic conditions,
99 which is highly regarded as pre-seismic precursor. Using more than 6 years observation
100 data of DEMETER, Zhang et al. (2013) found that there are increases in the number of
101 electron bursts events prior to the seismic activities; during the entire operation period of
102 the DEMETER satellite, along with electron burst precipitation occurred before each
103 strong earthquake with magnitude over 7.0. Ionospheric electromagnetic perturbations
104 were found by Zhima et al. (2012) 4 days before the earthquake in the ELF/VLF
105 frequency range. With the plasma data from DEMETER, Tao et al. (2017) found that both
106 the electron density (Ne) and ion density (Ni) pronouncedly increased, the O^+ density
107 increased and H^+density decreased while the He^+density remained relatively stable 2
108 days before the Java M7.7 earthquake in 2006.

Due to the importance and promising prospect of research about pre-seismic ionospheric anomalies, China Seismo-Electromagnetic Satellite (CSES) was launched on February 2, 2018 to monitor and study the seismic-ionospheric perturbations, and analyze the features of seismic-ionospheric perturbations. Several significant results were found during its first two years in orbit. With CSES data, Yan et al. (2018) studied 4 $M_w \geq 7.0$ earthquakes in 2018 and their results indicated unusual positive ionospheric perturbations in electron density, electron flux, VLF spectrogram, ion density and ion drift velocity 1-10 days before the studied earthquakes. It is also revealed by Song et al. (2020) that pre-seismic anomalies in electron density and total electron content (TEC) before 4 $M_w \geq 5.0$ earthquakes in 2018 by cross-validation analyzing the data from CSES, IRI-2016 model and total electron content (TEC) data from Center for Orbit Determination in Europe (CODE). In this paper, in order to analyze the features of seismic-ionospheric anomalies, but also to further verify the reliability of CSES scientific observation data, we investigated the seismic-ionospheric perturbations associated with the 14 July 2019 M_w7.2 Laiwui earthquake by cross-validation analyzing the GPS TEC data and data from different payloads of CSES (LAP and PAP). The basic information about seismic event and GPS satellite, CSES are briefly introduced in Section 2. The methodology and research results are presented in Section 3. In the end, discussion and conclusions of this study are implemented in Section 4.

2. Basic Information

2.1 Seismic Event Information

Indonesia is one of the most seismically active regions in the world, with comparatively much higher probability of seismic events occurrences. The frequent occurrence of earthquakes in this area provides an excellent chance and condition to study the phenomenon of seismic-ionospheric anomalies. Consequently, in this paper we took the Indonesian Laiwui earthquake occurred on 14 July 2019 as our research example. The magnitude M_w7.2 earthquake occurred in Indonesia Laiwui (-0.52°S, 128.17°E) with 10 km in depth at 09:10 UT (universal time) on 14 July 2019. The radius of the Laiwui earthquake preparation zone estimated by the Dorbrovosky formula $\rho = 10^{0.43M}$ is about 1247.38 km. Figure 1 shows the location of the earthquake epicenter and preparation zone on the map.

2.2 GPS Satellite Data

The GPS satellites transmit two L-band signals at the frequencies of 1575.42 and 1227.60 MHz and offer an effective method for monitoring the ionosphere. The TEC is a measure of the total number of electrons that would be contained in a cylinder that extends up vertically above a given point on the Earth all the way through the ionosphere. The network of GPS receivers can be used to simultaneously and continuously monitor the TEC. (Liu et al. 2004)

To investigate the TEC variations, the GIM data provided by NASA Jet Propulsion

148 Laboratory (JPL) were adopted to this study. The GIM is constructed into $5^{\circ} \times 2.5^{\circ}$
149 (Longitude, Latitude) grid with time resolution of 2 hour. GIM data are generated using
150 data from 150 GPS sites of the IGS and other institutions. In our study, the TEC data
151 based on the date and geographic location of Laiwui earthquake from 75 days before to
152 10 days after (30 April 2019 to 24 July 2019) the main shock occurred.

153 2.3 China Seismo-Electromagnetic Satellite Data

154 The China Seismo-Electromagnetic Satellite (CSES), which is also named as Zhang
155 Heng-1 (ZH-1), was successfully launched on February 2, 2018. The CSES is the first
156 space-based platform in China for both earthquake observation and geophysical field
157 measurement, and it is a sun-synchronous satellite orbiting at a height of approximately
158 507 km with a descending node of 14:00 local time, an ascending node time of 02:00 LT
159 with an inclination of 97.4°. The distance between its neighboring tracks is 2650 km (24°
160 in longitude) in one day, while reduced to 530 km (4° in longitude) in a revisit period of
161 5 days (Yan et al. 2018). The main objectives of this mission are to monitor the near-Earth
162 space environment and investigate possible electromagnetic perturbations related to
163 natural disasters and human activities. (Shen et al. 2018)

164 The scientific payload of the CSES is composed of several instruments that provide
165 a nearly continuous survey of ionospheric plasma, waves, and energetic particles. In this
166 study, the electron density and electron temperature data derived from LAP (Langmuir
167 Probe), ion density (He^{+}, O^{+}) and ion temperature data derived from PAP (Plasma
168 Analyzer Package) were applied to this research. Besides, also as shown in Figure 1 there

were about 100 flight orbits (most are revisited and overlapped orbits) above the earthquake region from one month before to 10 days after the earthquake (14 June to 24 July, 2019), which provided a significant amount of scientific observation data to our study. All the instrument data of CSES are available and can be obtained from www.leos.ac.cn

3. Methodology and Research Results

3.1 TEC anomalies

The moving median and inter-quartile scope of data are used to shape the upper and lower bounds so that the seismic-anomalies could be separated from the background (Liu et al.,2004). In addition, to calculate the statistical parameters, the length of the period was selected as about 55 days in order to avoid affects by the seasonal variations. (Richard et al., 2001; Liu et al., 2004; Cai et al., 2007; Liu et al., 2009; Liu et al., 2009; Akhoondazeh et al., 2010; Olwendo et al., 2012; Elemo et al., 2018). The upper and lower bound of the mentioned range can be calculated using the following equations (1)-(4):

$$TEC_{\mathrm{UB}} = TEC_{M30} + k \cdot TEC_{IQR} \quad (1)$$

$$TEC_{\mathrm{LB}} = TEC_{M30} - k \cdot TEC_{IQR} \quad (2)$$

$$\Delta TEC = \frac{(TEC_{obs} - TEC_{M30})}{\mathrm{TEC}_{IQR}} \quad (3)$$

$$\mathrm{p} = \pm[(\Delta TEC - \mathrm{k})/\mathrm{k}] \cdot 100\% \quad (4)$$

where TEC_{M30}, TEC_{IQR}, TEC_{UB}, TEC_{LB}, TEC_{obs}, ΔTEC and k are the 30-day

188 TEC moving median value, TEC inter-quartile range, TEC upper bound, TEC lower
189 bound, TEC observed value, differential of TEC and threshold of the anomaly,
190 respectively. Here we set the $k = 2.0$ considering the magnitude of the main shock to
191 select the anomalies interval. The value K must be dependent on the earthquake
192 magnitude as K would increase with earthquake magnitude. For instance, in big seismic
193 events with magnitude above 7.0, K can be chosen equal or above 2.0. For the K value
194 adopted in the manuscript, we referred to the methods in the following papers such as
195 Akhoondzadeh et al. (2010; 2011; 2012; 2013), Liu et al. (2000; 2001; 2004; 2009; 2011),
196 Tao et al., (2017), Akpan et al., (2019). Over and above, while the absolute value of
197 ΔTEC is larger than the k value ($|\Delta TEC| \geq k$), the behavior of the pertinent TEC value
198 will be noted as anomalous.

199 Basically, we check the variations of the geomagnetic data including Dst, Kp index
200 and solar flux F10.7 index variation during 30 May to 24 July 2019, i.e., 45 days before
201 to 10 days after the M_w7.2 Laiwui earthquake. Furthermore, a harsh condition (Dst > −30
202 nT, Kp < 3 and F10.7 < 100 sfu) is adopted to distinguish pre-seismic ionospheric
203 phenomena triggered by solar activities. Figure 2 shows that geomagnetic and solar
204 activities are relatively weak and quiet during that period except a magnetic storm
205 occurred on 10 July 2019, which is marked by red arrows and dashed elliptic. By a linear
206 interpolation of 4 data points which is adjacent the epicenter (0.52°S, 128.17°E), we
207 calculate the TEC above the epicenter. In consideration of the resolutions of the latitude
208 and longitude(2.5°in latitude and 5°in longitude) in GIM TEC , the ranges of 125° −

209 130°E and $0-2.5^{\circ}$ S are selected as the data points center. Seen from Figure 2d, it
210 represents the ΔTEC values between 30 May 2019 and 24 July 2019 according to
211 Equation (3).

212 In addition, anomalous TEC times are picked searched with $|\Delta TEC|$>2.0, Dst>−
213 30nT, Kp<3 and F10.7<100 sfu. The anomalies are found in 8 days (6 July) before the
214 earthquake, 3 days (11 July) before the earthquake, 1 day (13 July) before the earthquake
215 and 6 days after the earthquake (the main shock onset marked with a red star) illustrated
216 in Figure 2d. Likewise, the anomalies can be positive as well as negative which are
217 consistent with previous researches (Akhoondzadeh et al., 2010; Pulinets and Davidenko,
218 2014; Pulinets et al., 2003, 2015). We conclude there are increases of TEC anomaly
219 during the interval of 06:00-08:00 UT 6 July (i.e. 15:00-17:00 LT, +22.28% enhances),
220 08:00-10:00 UT 11 July (i.e. 17:00-19:00 LT, +13.85% enhances), 06:00-08:00 UT 13
221 July (i.e. 15:00-17:00 LT, +24.52% enhances) and decrease of TEC anomaly during the
222 interval of 16:00-18:00 UT 20 July (i.e. 01:00-03:00 LT, 22.75% decreases) according to
223 Equation (4).

224 3.2 Geographical anomalies on TEC with latitude-longitude-time (LLT) maps

225 With regarding to aforesaid four anomalous intervals, there is a geographical
226 investigation to check whether the GIM TEC concurrently disturbs in that earthquake
227 locality. Respectively, every GIM map consists of 5183 (71 * 73) grids and covers ±87.5°
228 N latitude and ±180°E longitude ranges with spatial resolutions of 2.5°in latitude and

229 5°in longitude.

230 As seen in Figure 3a, the column of GIM TECs LLT map is for each anomalous
231 interval (06:00-08:00 UT 6 July, 08:00-10:00 UT 11 July, 06:00-08:00 UT 13 July and
232 16:00-18:00 UT 20 July). The median of each grids on GIM TECs in each anomalous
233 above-mentioned interval during 1-30 days before each anomalous interval is shown in
234 Figure 3b. Figure 3c shows ultimate difference of TEC ($|\Delta TEC| \geq 2.0$) between the
235 observed GIM TEC and the associated 30-day median at four anomalous intervals
236 occurred on 06:00-08:00 UT 6 July (1st column), 08:00-10:00 UT 11 July (2nd column),
237 06:00-08:00 UT 13 July (3rd column) and 16:00-18:00 UT 20 July (4th column),
238 respectively. Generally, the 30-day median is on behalf of the undisturbed background,
239 whereas positive difference of TEC represents the enhancement of GIM TECs but
240 negative difference of TEC represents the decrease of GIM TECs.

241 As shown in Figure 3c, the GIM TECs around Laiwui earthquake epicenter
242 dramatically enhance by ~1.14-31.03% in the interval of 06:00-08:00 UT 6 July (15:00-
243 17:00 LT), ~0.75-56.98% in the interval of 08:00-10:00 UT 11 July (17:00-19:00 LT),
244 ~2.75-66.68% in the interval of 06:00-08:00 UT 13 July (15:00-17:00 LT) and decrease
245 by ~3.40-32.50% in the interval of 06:00-08:00 UT 13 July (15:00-17:00 LT),
246 ~2.70~41.38% in the interval of 16:00-18:00 UT 20 July (01:00-03:00 LT).

247 The sequence of GIM for four corresponding global fixed local times was examined
248 in exchange for eliminating the local time and/or EIA effects. As shown in Figure 3
249 compared with the TEC enhancements at four different universal times in Figure 4, the

corresponding extreme enhancements in the GIM TECs at global fixed local times are also chiefly positioned around the forthcoming epicenter and EIA region. Accordingly, the geographical anomalies simultaneously and remarkably appear in the four anomalous intervals around the epicenter of the Laiwui earthquake. Concretely, the GIM TECs around Laiwui earthquake epicenter dramatically enhance by ~6.98-65.31% in the interval of 06:00-08:00 UT 6 July (15:00-17:00 LT), ~0.45-19.28% in the interval of 08:00-10:00 UT 11 July (17:00-19:00 LT), ~10.00-62.16% in the interval of 06:00-08:00 UT 13 July (15:00-17:00 LT) and decrease by ~5.88-23.53% in the interval of 16:00-18:00 UT 20 July (01:00-03:00 LT). The results of global fixed local time GIM TEC spatial distributions are indeed consistent with the TEC temporal anomalies analysis presented in subsection 3.1.

3.3 Plasma parameters perturbations

In this study, GIM TEC anomalies derived from GPS satellites 45 days before to 10 days after the earthquake have been analyzed. To confirm the observed TEC anomalies further, a cross-valid examination was conducted with the application of the observation data from CSES.

As introduced in subsection 2.3, the data recorded by payloads LAP and PAP on CSES are adopted to study the ionospheric plasma parameters perturbations above the earthquake preparation zone during the period of 30 days before (14 June 2019) to 5 days after (19 July 2019) the Laiwui earthquake. We examine the percentage deviation of the plasma parameters recorded by CSES within 30 days before and 10 days after the

earthquake via moving mean method. Deviation of the plasma parameters can be calculated by using the following equations:

$$dN = \frac{N_{obs} - N_{mean}}{N_{mean}} \times 100\% \quad (5)$$

$$dT = \frac{T_{obs} - T_{mean}}{T_{mean}} \times 100\% \quad (6)$$

where N_{obs} and T_{obs} are the CSES observed values for each plasma parameter, while N_{mean} and T_{mean} are perceived as the background values, which are the corresponding moving means from previous 30 days orbit data (data cell is sampled by 2° in latitude and 4° in longitude). To be more specific, the average values for each parameter of different orbits were calculated using the data from 30 days before the orbit date. Indeed, unusual perturbations in different ionospheric plasma parameters are detected prior to 14 July Laiwui earthquake. Figure 5a-e displays the percentage deviation of electron density (*Ne*), electron temperature (T_e), O^+ density (N_{O^+}), ion temperature (T_i) and He^+ density (N_{He^+}) respectively. However, due to the measurement limitation of the PAP instrument, there is little valid data for H^+ density above the earthquake area and the measurement of He^+ density is also not persistent for some certain orbits.

From the TEC anomalies analysis, the TEC anomalies were detected on 8 days (6 July), 3 days (11 July) and 1 day (13 July) prior to the earthquake. A further cross-valid analysis is conducted during these periods. As shown in Figure 5a, the electron density increased significantly on day 4 (10 July) and day 2 (12 July) before the earthquake, the maximum value increased by approximately 135.32% and 115.69% respectively when it

291 approached the epicenter. While, on day 3 (11 July) and day1 (13 July) before the
292 earthquake, the maximum only increased by about 16.80% and 39.58%. Similarly, as
293 shown in Figure 5c the main component O^+ density also increased dramatically on day
294 4 (10 July) and day 2 (12 July) before the seismic event when it approached the epicenter,
295 the maximum value increased by 160.10% and 153.74% respectively. While, the O^+
296 density remained relatively stable 3 days before and 1 day before with a slight increase
297 about 10.63% and 21.73%. Although the observation data of He^+ density is not
298 persistent for some orbits, as shown in Figure 5e, the variation tendency of He^+ density
299 can still be observed from the data recorded by CSES. He^+ density profoundly
300 increased when flying above the epicenter on 4 days before the earthquake with maximum
301 increased by 154.76%. The electron temperature and the ion temperature, however,
302 remained relatively stable during the observation period, with a comparatively slight
303 increase no more than 60% for all orbits.

304 Also, Figure 6a-e displays the percentage deviation of the same plasma parameters,
305 while the observation period is from 4 July to 8 July. Since a magnetic storm occurred on
306 10 July, as shown in Figure 2, it is difficult to distinguish whether the anomalies on 10
307 July is caused by the magnetic storm or the earthquake. As displayed in Figure 6a, the
308 electron density dramatically increased on 5 July and 7 July when approaching the
309 epicenter with a maximum increase by approximately 129.29% and 151.17% respectively.
310 While the electron density on 4 July and 6 July remained relatively stable, with the
311 greatest deviation percentage no more than 80%. O^+ density increased significantly by

312 the order of 112.61% and 197.77% on 5 July and 7 July, while the adjacent orbits
313 remained relatively stable. Besides, He^+ density also increased simultaneously with the
314 O^+ density on 7 July, with a maximum increase by 186.29% Furthermore, the variation
315 of the electron and ion temperature still remained relatively stable (deviation no more
316 than 50%) without significant perturbations during the observation period.

317 To further verify the unusual variations of the in-situ parameters further, the electron
318 density (Ne) and electron temperature (Te) data of the abnormal orbits were extracted to
319 make comparation with their corresponding revisited orbits. Figure 7a and b represent the
320 variation of electron density of 12 July and 10 July along with their corresponding
321 revisited orbits. It can be clearly observed that the electron density increased significantly
322 within $0^\circ - 20^\circ$N, with a peak value reaching $9.21\times 10^{10} N_e/m^3$, $9.59\times 10^{10} N_e/m^3$ on
323 12 July and 10 July respectively. Although due to the equator ionospheric anomaly (EIA),
324 the electron density all increased near the magnetic equator (7.6°N), it can still be
325 observed that the abnormal orbits did show unusual positive anomalies, compared with
326 their corresponding revisited orbits. Figure 7c and d demonstrate the change of electron
327 temperature of the same orbits, and it is presented in the results that Te is inversely
328 proportional to Ne. This phenomenon is caused by the cooling process of electrons, of
329 which the rate is proportional to the square of Ne and consistent with the basic ionospheric
330 theory concerning the relationship between these two parameters. ((Bilitza, 1975; Bilitza
331 and Hoegy, 1990; Kakinami et al., 2011; Song et al., 2020)

332 Furthermore, it also should be noted that CSES usually flew above the earthquake

preparation zone twice a day, with a descending orbit and an ascending orbit respectively. The obvious disturbances were observed by CSES when it was flying above the region with descending orbits. However, we do not find any similar variations in plasma parameters before the occurrence of earthquake during ascending orbits at about 17:00 UT (02:00 LT)

4. Discussion and Conclusion

In this study, seismic-ionospheric anomalies associated with the M_w7.2 Laiwui earthquake were comprehensively investigated. Regarding the temporal distribution, from the observation of the GPS satellite, there were three significant positive perturbations in TEC 1, 3, 8 days prior to the earthquake and a negative disturbance 6 days after the earthquake under the relatively quiet geomagnetic conditions. In respect of the spatial distribution, considering the local time and EIA effects, the spatial distribution and the signs of the anomalies agree well with those of the TEC anomalies (Figure 2d) on each day. To make the results more convincing, more extended types of investigations were carried out, such as in-situ investigations of plasma parameters variations using the data from LAP, PAP of CSES. All the results of these investigations indicate the seismic-ionospheric anomalies prior to the Laiwui earthquake. It should be noted that the unusual TEC perturbations on 7 July may also be associated with the M_w6.9 earthquake, which occurred on 7 July in Kota Ternate (0.513°N, 126.19°E) near the epicenter.

Nevertheless, further discussions are required for some of the results. A cross-valid analysis of TEC anomalies was conducted using the LAP and PAP data of CSES, and the

354 results are indeed consistent with the former one. There were great enhancements in
355 plasma parameters (electron density, ion density, etc.) prior to the earthquake, however,
356 there was also a difference between the two results. For example, the most significant
357 anomalies of the electron density were observed on day 4 (10 July) and day 2 (12 July)
358 before the earthquake, while the TEC anomalies were exactly one day after the CSES
359 observations. Besides, a negative anomaly in TEC was also detected 6 days after the
360 earthquake, but similar disturbances were not detected by CSES. There might be several
361 reasons accounting for these discrepancies, on the one hand, as shown in Figure 4b, the
362 Kp index increased at 4:00-10:00 UT on 10 July, while the electron density also increased
363 simultaneously during the same period, so the disturbances on 10 July may be related to
364 the geomagnetic activity. On the other hand, the discrepancies may be mainly attributed
365 to the difference of the two datasets. To be specific, CSES is a spacecraft exploring the
366 topside ionosphere at an altitude about 507 km with in-situ observations, while the GPS-
367 TEC is calculated under the assumption of the ionospheric single layer.

368 Besides, some of the TEC anomalies were observed outside the preparation zone.,
369 as shown in Figure 3 and Figure 4. This can be attributed to lithosphere-atmosphere-
370 ionosphere coupling (LAIC) process, the Dobrovolsky formula is an ideal equation
371 without the consideration of the LAIC process. The earthquake-related anomalies induced
372 by the LAIC mechanism works complicatedly, whose wave channels mainly is composed
373 of the acoustic-gravity wave (AGW) propagation, electromagnetic emission (EME) and
374 geochemical channel (Pulinets and Boyarchuk, 2004; Kamogawa, 2006; Hayakawa, 2006;

375 Kuo et al., 2014; Pulinets and Davidenko, 2014). Therefore, the seismic-ionospheric
376 anomalies may propagate to further distance.

377 As for the observation discrepancies in different CSES orbits (ascending and
378 descending ones), this may be attributed to the ionospheric daily variation. The
379 descending orbits of the CSES usually flew above the earthquake region at about 15:00
380 LT (06:00 UT), while the ascending orbits passed there at about 02:00 LT (17:00UT). At
381 daytime, the ionosphere received much more radiation from the sun resulting in more
382 ionized particles, which significantly increases the density of the ionospheric electrons
383 and ions. While the densities of the electrons and ions are much lower at night time. Due
384 to the relatively lower electron and ion densities, the variations of the ionospheric plasma
385 parameters will be much more difficult to be detected by CSES. Thus, the plasma
386 parameters observed by CSES remained relatively stable during nighttime prior to the
387 earthquake. Also, perturbations in electron density occurred more often than those of
388 electron temperature from the observation results of CSES, which illustrate that electron
389 density is much more sensitive to seismic activity than electron temperature, this is also
390 consistent with the statistical investigation conducted by Liu et al. (2014). Besides, it also
391 should be noted that the PAP instrument of CSES is slightly contaminated, with lower
392 absolute value in observation data, therefore the data of PAP can only be applied to the
393 relative deviation analysis.

394 In conclusion, during these periods, the measurements of GPS and CSES yield
395 similar tendencies, the temporal and spatial anomalies of the TEC and ionospheric plasma

perturbations detected by CSES over the epicenter did indicate significant positive seismic-ionospheric anomalies. Based on the results presented, we can also safely draw the conclusion that CSES data are reliable for the study of seismic events. Also, the localization and synchronization of the longtime anomalies around the occurrence of earthquake suggest that these perturbations are highly associated with M_w7.2 Laiwui earthquake, but further investigations are required in the future to obtain a more accurate knowledge of the perturbation process.

Supplementary materials

The 55 days day to day TEC data are provided as supplementary figure 1, other CSES orbits with plasma parameters variations are provided as supplementary figure 2 and 3.

List of abbreviations

TEC: Total Electron Content

CSES: China Seismo-Electromagnetic Satellite

LAP: Langmuir Probe

PAP: Plasma Analyzer Package

Availability of data and materials

OMNI and GPS data are available from https://cdaweb.gsfc.nasa.gov/sp_phys/. CSES data are accessible from http://www.leos.ac.cn. All earthquake data are available from https: //earthquake.usgs.gov/earthquakes.

Competing interests

The authors declare that they have no competing interests.

Funding

This work was supported by the National Natural Science Foundation of China (NSFC) under Grant No. 42004137.

Acknowledgements

We acknowledge use of GPS TEC data provided by NASA Jet Propulsion Laboratory (JPL) and CSES data available from http://www.leos.ac.cn . We also thank the National Earthquake Information Center (NEIC) ComCat database of the US Geological Survey for providing available earthquake data. The authors would like to thank Dr. Rui Yan at the Institute of Crustal Dynamics and Mr. Hongyi Fu at Chengdu University of Technology for helpful discussions. The authors also would like to thank Mr. Hengxin Lu and Mr. Dapeng Liu at CSES ground application center for the CSES data services. This work was supported by the National Natural Science Foundation of China (NSFC) under Grant No. 42004137.

Authors' information

1. Key Laboratory of Earth Exploration and Information Techniques of Ministry of Education of China, Chengdu University of Technology, Chengdu, China

2. College of Geophysics, Chengdu University of Technology, Chengdu, China

3. School of Space and Environment, Beihang University, Beijing, China

4. Dipartimento di Fisica, Università di Trento, Trento, Italy

5. National Institute of Natural Hazards, Ministry of Emergency Management of China, Beijing, China

References:

1. Akhoondzadeh M. (2012). Anomalous TEC variations associated with the powerful Tohoku earthquake of 11 March 2011. Nat. Hazards Earth Syst. Sci., 12(5), 1453-1462. doi: 10.5194/nhess-12-1453-2012

2. Akhoondzadeh M. (2013). A MLP neural network as an investigator of TEC time series to detect seismo-ionospheric anomalies. ADV SPACE RES, 51(11), 2048-2057. doi: https://doi.org/10.1016/j.asr.2013.01.012

447 3. Akhoondzadeh M, Parrot M, Saradjian MR. (2010). Electron and ion
448 density variations before strong earthquakes (M>6.0) using DEMETER and
449 GPS data. Nat. Hazards Earth Syst. Sci., 10(1), 7-18. doi: 10.5194/nhess-10-
450 7-2010

451 4. Akhoondzadeh M, Saradjian MR. (2011). TEC variations analysis
452 concerning Haiti (January 12, 2010) and Samoa (September 29, 2009)
453 earthquakes. ADV SPACE RES, 47(1), 94-104. doi:
454 https://doi.org/10.1016/j.asr.2010.07.024

455 5. Akpan AE, Ibanga JI, George NJ, Ekanem AM. (2019). Assessing
456 seismo-ionospheric disturbances using Vanuatu and Honshu earthquakes of
457 March 25, 2007, employing DEMETER and GPS data. INT J ENVIRON SCI
458 TE, 16(11), 7187-7196. doi: 10.1007/s13762-019-02339-x

459 6. Bilitza D. (1975). Models for the relationship between electron density
460 and temperature in the upper ionosphere. Journal of Atmospheric and
461 Terrestrial Physics, 37(9), 1219-1222. doi: https://doi.org/10.1016/0021-
462 9169(75)90193-2

463 7. Bilitza D, Hoegy WR. (1990). Solar activity variation of ionospheric
464 plasma temperatures. ADV SPACE RES, 10(8), 81-90. doi:
465 https://doi.org/10.1016/0273-1177(90)90190-B

466 8. Cai C. (2007). Monitoring seasonal variations of ionospheric TEC
467 using GPS measurements. Geo-spatial information science, 10(2), 96-99. doi:
468 10.1007/s11806-007-0034-z

469 9. De Santis A, De Franceschi G, Spogli L, Perrone L, Alfonsi L, Qamili
470 E, Cianchini G, Di Giovambattista R, Salvi S, Filippi E, Pavón-Carrasco FJ,
471 Monna S, Piscini A, Battiston R, Vitale V, Picozza PG, Conti L, Parrot M,
472 Pinçon JL, Balasis G, Tavani M, Argan A, Piano G, Rainone ML, Liu W, Tao
473 D. (2015). Geospace perturbations induced by the Earth: The state of the art
474 and future trends. Physics and Chemistry of the Earth, Parts A/B/C, 85-86,
475 17-33. doi: 10.1016/j.pce.2015.05.004

476 10. Elemo EO, Ehigiator MO, Ehigiator-Irughe R. (2018). Seasonal

477 variations of the Vertical Total Electron Content (VTEC) of the ionosphere at
478 the GNSS cor station (SEERL) UNIBEN and three other cors stations in
479 Nigeria. Nigerian Journal of Technology, 37(2), 286-293. doi:
480 10.4314/njt.v37i2.1

481 11. Hayakawa M, Itoh T, Hattori K, Yumoto K. (2000). ULF
482 electromagnetic precursors for an earthquake at Biak, Indonesia on February
483 17, 1996. GEOPHYS RES LETT, 27(10), 1531-1534. doi:
484 https://doi.org/10.1029/1999GL005432

485 12. Hayakawa M, Schekotov A, Izutsu J, Nickolaenko AP. (2019).
486 Seismogenic effects in ULF/ELF/VLF electromagnetic waves.
487 INTERNATIONAL JOURNAL OF ELECTRONICS AND APPLIED
488 RESEARCH, 06(02), 1-86. doi: 10.33665/IJEAR.2019.v06i02.001

489 13. Heki K. (2011). Ionospheric electron enhancement preceding the 2011
490 Tohoku-Oki earthquake. GEOPHYS RES LETT, 38(17). doi:
491 https://doi.org/10.1029/2011GL047908

492 14. Ho Y, Jhuang H, Su Y, Liu J. (2013). Seismo-ionospheric anomalies in
493 total electron content of the GIM and electron density of DEMETER before
494 the 27 February 2010 M8.8 Chile earthquake. ADV SPACE RES, 51(12),
495 2309-2315. doi: 10.1016/j.asr.2013.02.006

496 15. Kakinami Y, Lin CH, Liu JY, Kamogawa M, Watanabe S, Parrot M.
497 (2011). Daytime longitudinal structures of electron density and temperature
498 in the topside ionosphere observed by the Hinotori and DEMETER satellites.
499 Journal of Geophysical Research: Space Physics, 116(A5). doi:
500 10.1029/2010JA015632

501 16. Kamogawa M. (2006). Preseismic lithosphere-atmosphere-ionosphere
502 coupling. Eos, Transactions American Geophysical Union, 87(40), 417-424.
503 doi: https://doi.org/10.1029/2006EO400002

504 17. Kon S, Nishihashi M, Hattori K. (2011). Ionospheric anomalies
505 possibly associated with M⩾6.0 earthquakes in the Japan area during 1998-
506 2010: Case studies and statistical study. J ASIAN EARTH SCI, 41(4-5), 410-

507 420. doi: 10.1016/j.jseaes.2010.10.005

508 18. Kuo CL, Huba JD, Joyce G, Lee LC. (2011). Ionosphere plasma
509 bubbles and density variations induced by pre-earthquake rock currents and
510 associated surface charges. Journal of Geophysical Research: Space Physics,
511 116(A10). doi: https://doi.org/10.1029/2011JA016628

512 19. Kuo CL, Lee LC, Huba JD. (2014). An improved coupling model for
513 the lithosphere-atmosphere-ionosphere system. Journal of Geophysical
514 Research: Space Physics, 119(4), 3189-3205. doi: 10.1002/2013JA019392

515 20. Liu J, Chen C, Lin C, Tsai H, Chen C, Kamogawa M. (2011).
516 Ionospheric disturbances triggered by the 11 March 2011 M9.0 Tohoku
517 earthquake. Journal of Geophysical Research: Space Physics, 116(A6). doi:
518 https://doi.org/10.1029/2011JA016761

519 21. Liu J, Huang J, Zhang X. (2014). Ionospheric perturbations in plasma
520 parameters before global strong earthquakes. ADV SPACE RES, 53(5), 776-
521 787. doi: 10.1016/j.asr.2013.12.029

522 22. Liu JY, Chen YI, Chen CH, Liu CY, Chen CY, Nishihashi M, Li JZ,
523 Xia YQ, Oyama KI, Hattori K, Lin CH. (2009). Seismoionospheric GPS total
524 electron content anomalies observed before the 12 May 2008Mw7.9
525 Wenchuan earthquake. Journal of Geophysical Research: Space Physics,
526 114(A4), n/a-n/a. doi: 10.1029/2008JA013698

527 23. Liu JY, Chen YI, Chuo YJ, Tsai HF. (2001). Variations of ionospheric
528 total electron content during the Chi-Chi Earthquake. GEOPHYS RES LETT,
529 28(7), 1383-1386. doi: https://doi.org/10.1029/2000GL012511

530 24. Liu JY, Chen YI, Huang CC, Parrot M, Shen XH, Pulinets SA, Yang
531 QS, Ho YY. (2015). A spatial analysis on seismo-ionospheric anomalies
532 observed by DEMETER during the 2008 M8.0 Wenchuan earthquake. J
533 ASIAN EARTH SCI, 114, 414-419. doi: 10.1016/j.jseaes.2015.06.012

534 25. Liu JY, Chen YI, Pulinets SA, Tsai YB, Chuo YJ. (2000). Seismo-
535 ionospheric signatures prior to M≥6.0 Taiwan earthquakes. GEOPHYS RES

536 LETT, 27(19), 3113-3116. doi: https://doi.org/10.1029/2000GL011395

537 26. Liu JY, Chuo YJ, Shan SJ, Tsai YB, Chen YI, Pulinets SA, Yu SB.
538 (2004). Pre-earthquake ionospheric anomalies registered by continuous GPS
539 TEC measurements. Ann. Geophys., 22(5), 1585-1593. doi: 10.5194/angeo-22-
540 1585-2004

541 27. Liu JY, Le H, Chen YI, Chen CH, Liu L, Wan W, Su YZ, Sun YY, Lin
542 CH, Chen MQ. (2011). Observations and simulations of seismoionospheric
543 GPS total electron content anomalies before the 12 January 2010 M7 Haiti
544 earthquake. Journal of Geophysical Research: Space Physics, 116(A4). doi:
545 https://doi.org/10.1029/2010JA015704

546 28. Liu JY, Tsai YB, Chen SW, Lee CP, Chen YC, Yen HY, Chang WY, Liu
547 C. (2006). Giant ionospheric disturbances excited by the M9.3 Sumatra
548 earthquake of 26 December 2004. GEOPHYS RES LETT, 33(2). doi:
549 10.1029/2005GL023963

550 29. Liu JY, Tsai YB, Chen SW, Lee CP, Chen YC, Yen HY, Chang WY, Liu
551 C. (2006). Giant ionospheric disturbances excited by the M9.3 Sumatra
552 earthquake of 26 December 2004. GEOPHYS RES LETT, 33(2). doi:
553 https://doi.org/10.1029/2005GL023963

554 30. Liu L, Chen Y. (2009). Statistical analysis of solar activity variations
555 of total electron content derived at Jet Propulsion Laboratory from GPS
556 observations. Journal of Geophysical Research: Space Physics, 114(A10), n/a-
557 n/a. doi: 10.1029/2009JA014533

558 31. Liu L, Zhao B, Wan W, Ning B, Zhang M, He M. (2009). Seasonal
559 variations of the ionospheric electron densities retrieved from Constellation
560 Observing System for Meteorology, Ionosphere, and Climate mission radio
561 occultation measurements. Journal of Geophysical Research: Space Physics,
562 114(A2), n/a-n/a. doi: 10.1029/2008JA013819

563 32. Ogwala A, Somoye EO, Ogunmodimu O, Adeniji-Adele RA, Onori EO,
564 Oyedokun O. (2019). Diurnal, seasonal and solar cycle variation in total
565 electron content and comparison with IRI-2016 model at Birnin Kebbi. ANN

566 GEOPHYS-GERMANY, 37(5), 775-789. doi: 10.5194/angeo-37-775-2019

567 33. Olwendo OJ, Baki P, Mito C, Doherty P. (2012). Characterization of
568 ionospheric GPS Total Electron Content (GPS-TEC) in low latitude zone over
569 the Kenyan region during a very low solar activity phase. J ATMOS SOL-
570 TERR PHY, 84-85, 52-61. doi: 10.1016/j.jastp.2012.06.003

571 34. Pulinets S, Davidenko D. (2014). Ionospheric precursors of
572 earthquakes and Global Electric Circuit. ADV SPACE RES, 53(5), 709-723.
573 doi: https://doi.org/10.1016/j.asr.2013.12.035

574 35. Pulinets S, Ouzounov D. (2011). Lithosphere - Atmosphere -
575 Ionosphere Coupling (LAIC) model - An unified concept for earthquake
576 precursors validation. J ASIAN EARTH SCI, 41(4), 371-382. doi:
577 https://doi.org/10.1016/j.jseaes.2010.03.005

578 36. Pulinetsl S. (2004). Ionospheric Precursors of Earthquakes; Recent
579 Advances in Theory and Practical Applications. TAO : Terrestrial,
580 atmospheric, and oceanic sciences, 15(3), 413. doi:
581 10.3319/TAO.2004.15.3.413(EP)

582 37. Richards PG. (2001). Seasonal and solar cycle variations of the
583 ionospheric peak electron density: Comparison of measurement and models.
584 Journal of Geophysical Research: Space Physics, 106(A7), 12803-12819. doi:
585 10.1029/2000JA000365

586 38. Shen X, Zhang X, Yuan S, Wang L, Cao J, Huang J, Zhu X, Piergiorgio
587 P, Dai J. (2018). The state-of-the-art of the China Seismo-Electromagnetic
588 Satellite mission. Science China Technological Sciences, 61(5), 634-642. doi:
589 10.1007/s11431-018-9242-0

590 39. Song R, Hattori K, Zhang X, Sanaka S. (2020). Seismic-ionospheric
591 effects prior to four earthquakes in Indonesia detected by the China seismo-
592 electromagnetic satellite. J ATMOS SOL-TERR PHY, 205, 105291. doi:
593 10.1016/j.jastp.2020.105291

594 40. Sorokin VM, Chmyrev VM, Yaschenko AK. (2001). Electrodynamic

595 model of the lower atmosphere and the ionosphere coupling. J ATMOS SOL-
596 TERR PHY, 63(16), 1681-1691. doi: https://doi.org/10.1016/S1364-
597 6826(01)00047-5

598 41. Sorokin VM, Yaschenko AK, Hayakawa M. (2006). Formation
599 mechanism of the lower-ionospheric disturbances by the atmosphere electric
600 current over a seismic region. J ATMOS SOL-TERR PHY, 68(11), 1260-1268.
601 doi: https://doi.org/10.1016/j.jastp.2006.03.005

602 42. Tao D, Cao J, Battiston R, Li L, Ma Y, Liu W, Zhima Z, Wang L,
603 Dunlop MW. (2017). Seismo-ionospheric anomalies in ionospheric TEC and
604 plasma density before the 17 July 2006 M7.7 south of Java earthquake. ANN
605 GEOPHYS-GERMANY, 35(3), 589-598. doi: 10.5194/angeo-35-589-2017

606 43. Yan R, Shen X, Huang J, Wang Q, Chu W, Liu D, Yang Y, Lu H, Xu S.
607 (2018). Examples of unusual ionospheric observations by the CSES prior to
608 earthquakes. Earth and Planetary Physics, 2(6), 515-526. doi:
609 https://doi.org/10.26464/epp2018050

610 44. Zhang X, Chen H, Liu J, Shen X, Miao Y, Du X, Qian J. (2012).
611 Ground-based and satellite DC-ULF electric field anomalies around
612 Wenchuan M8.0 earthquake. ADV SPACE RES, 50(1), 85-95. doi:
613 https://doi.org/10.1016/j.asr.2012.03.018

614 45. Zhang X, Qian J, Ouyang X, Shen X, Cai JA, Zhao S. (2009).
615 Ionospheric electromagnetic perturbations observed on DEMETER satellite
616 before Chile M7.9 earthquake. Earthquake Science, 22(3), 251-255. doi:
617 10.1007/s11589-009-0251-7

618 46. Zhang X, Shen X, Liu J, Ouyang X, Qian J, Zhao S. (2010). Ionospheric
619 perturbations of electron density before the Wenchuan Earthquake. INT J
620 REMOTE SENS, 31(13), 3559-3569. doi: 10.1080/01431161003727762

621 47. Zhao B, Wang M, Yu T, Wan W, Lei J, Liu L, Ning B. (2008). Is an
622 unusual large enhancement of ionospheric electron density linked with the
623 2008 great Wenchuan earthquake? Journal of Geophysical Research: Space
624 Physics, 113(A11). doi: https://doi.org/10.1029/2008JA013613

625 48. Zhao S, Shen X, Pan W, Zhang X, Liao L. (2010). Penetration
626 characteristics of VLF wave from atmosphere into lower ionosphere.
627 Earthquake Science, 23(3), 275-281. doi: 10.1007/s11589-010-0723-9

628 49. Zhima Z, Xuhui S, Xuemin Z, Jinbin C, Jianping H, Xinyan O, Jing
629 L, Lu B. (2012). Possible Ionospheric Electromagnetic Perturbations Induced
630 by the Ms7.1 Yushu Earthquake. Earth, Moon, and Planets, 108(3-4), 231-
631 241. doi: 10.1007/s11038-012-9393-z

632

633

634

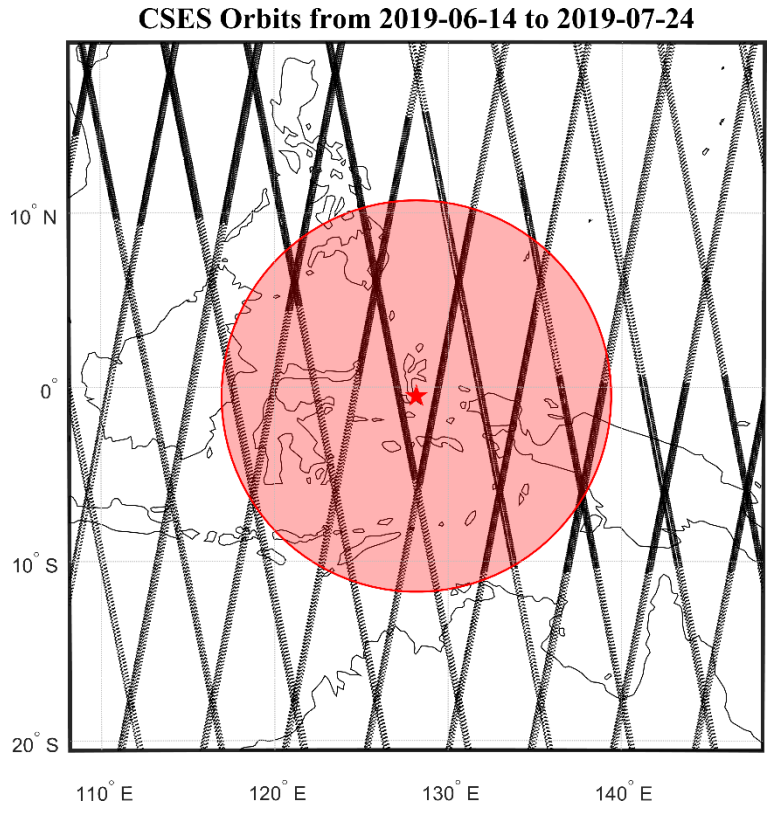

635

636 **Figure 1.** The red star and circle represent the epicenter and preparation zone of
637 M_w 7.2 Laiwui earthquake and the CSES orbits tracks from 2019-06-14 to 2019-07-24
638 are marked with black points.

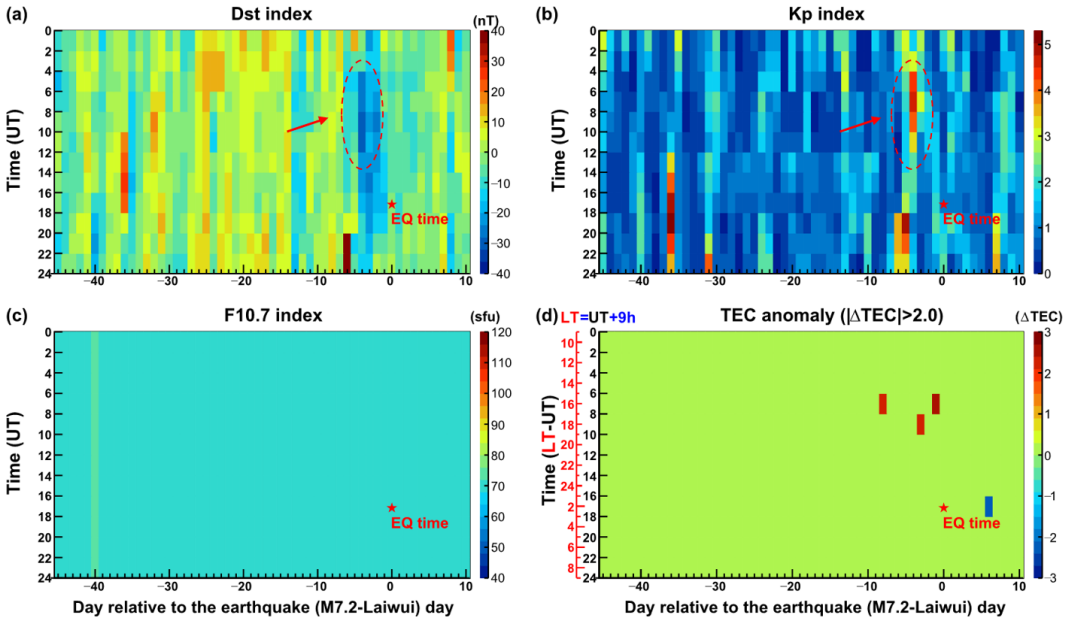

639

640 **Figure 2.** TEC anomaly analysis for the Laiwui earthquake (14 July 2019) from 30 May
641 2019 (45 days before the earthquake) to 24 July 2019 (10 days after the earthquake).
642 The earthquake time is represented by a red star. The x axis represents the day relative to
643 the earthquake day. The y axis represents the UT (LT = UT + 9 h). (a) Dst geomagnetic
644 index, the magnetic storm occurred on 10 July is marked with the red arrow and dashed
645 elliptic. (b) Kp geomagnetic index, the magnetic storm occurred on 10 July is marked
646 with the red arrow and dashed elliptic. (c) Solar radio flux F10.7 index. (d) TEC
647 anomalies detected under the following conditions: Dst > −30 nT, Kp < 3, F10.7 < 100
648 sfu and $|\Delta TEC| > 2.0$. Here 1 TECU = 10^{16}electrons$/m^2$.

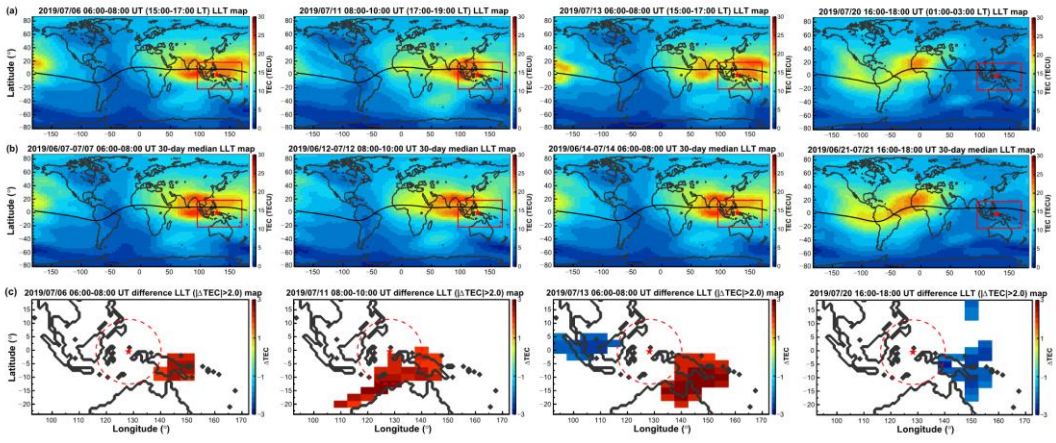

649

Figure 3. The GIM latitude-longitude-time (LLT) maps observed during the interval of 06:00-08:00 UT 6 July, 08:00-10:00 UT 11 July, 06:00-08:00 13 July before the 14 July 2019 M_w7.2 Laiwui earthquake and 16:00-18:00 UT 20 July after the14 July 2019 M_w7.2 Laiwui earthquake. The GIM LLT maps during the fixed period of 06:00–08:00 UT 6 July 2019 (1st column), 08:00–10:00 UT 11 July 2019 (2nd column), 06:00–08:00 UT 13 July 2019 (3rd column) and 16:00-18:00 UT 20 July 2019 (4th column). Panels of row (a) are the observed values on 8 days before the earthquake (6 July 2019), 3 days before the earthquake (11 July 2019), a day before the earthquake (13 July 2019) and 6 days after the earthquake (20 July 2019), while row (b) shows the median values of the period of days 1–30 before each anomalous interval. The red squares in rows (a, b) indicate the regions of interest around the earthquake, in range of 22°S–18°N latitude and 95°-170°E longitude. Panels of row (c) denote the extreme differences ($|\Delta TEC| >$ 2.0) of the 30-day period that appeared on 8 days before the earthquake (6 July 2019), 3 days before the earthquake (11 July 2019), a day before the earthquake (13 July 2019) and 6 days after the earthquake (20 July 2019) with the regions of interest around the earthquake. The color denotes the difference value of the TEC from the relevant median value. The red dashed circles with the radius ρ=1247.38km represent the earthquake preparation area of the lithosphere.

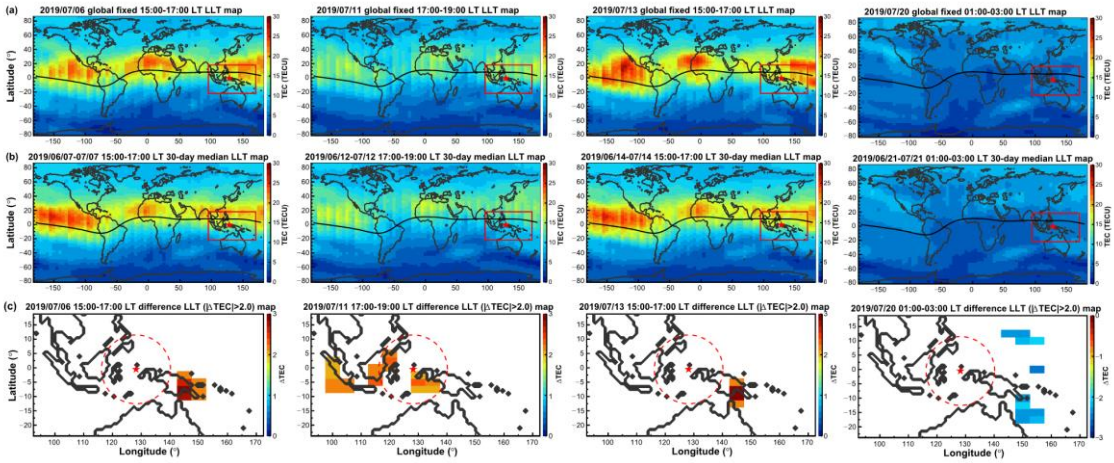

Figure 4. The GIM LLT maps observed during the global fixed intervals of 15:00-17:00 LT 6 July, 17:00-19:00 LT 11 July, 15:00-17:00 LT 13 July before the earthquake and 01:00-03:00 LT 20 July after the earthquake. The GIM LLT maps during four global fixed local times: (1st column) 15:00-17:00 LT 6 July 2019, (2nd column) 17:00-19:00 LT 11 July 2019, (3rd column) 15:00-17:00 LT 13 July 2019 and (4th column) 01:00-03:00 LT

20 July 2019, respectively. Panels of row (a) are the observed values on 8 days before the earthquake (6 July 2019), 3 days before the earthquake (11 July 2019), a day before the earthquake (13 July 2019), and 6 days after the earthquake (20 July 2019), while row (b) shows the median values of the period of days 1–30 before each anomalous interval. The red squares in rows (a, b) indicate the regions of interest around the earthquake, in range of 22°S–18°N latitude and 95°-170°E longitude. Panels of row (c) denote the extreme differences ($|\Delta TEC| > 2.0$) of the 30-day period that appeared on 8 days before the earthquake (6 July 2019), 3 days before the earthquake (11 July 2019), a day before the earthquake (13 July 2019) and 6 days after the earthquake (20 July 2019) with the regions of interest around the earthquake. The color denotes the difference value of the TEC from the relevant median value. The red dashed circles with the radius $\rho =$ 1247.38km represent the earthquake preparation zone.

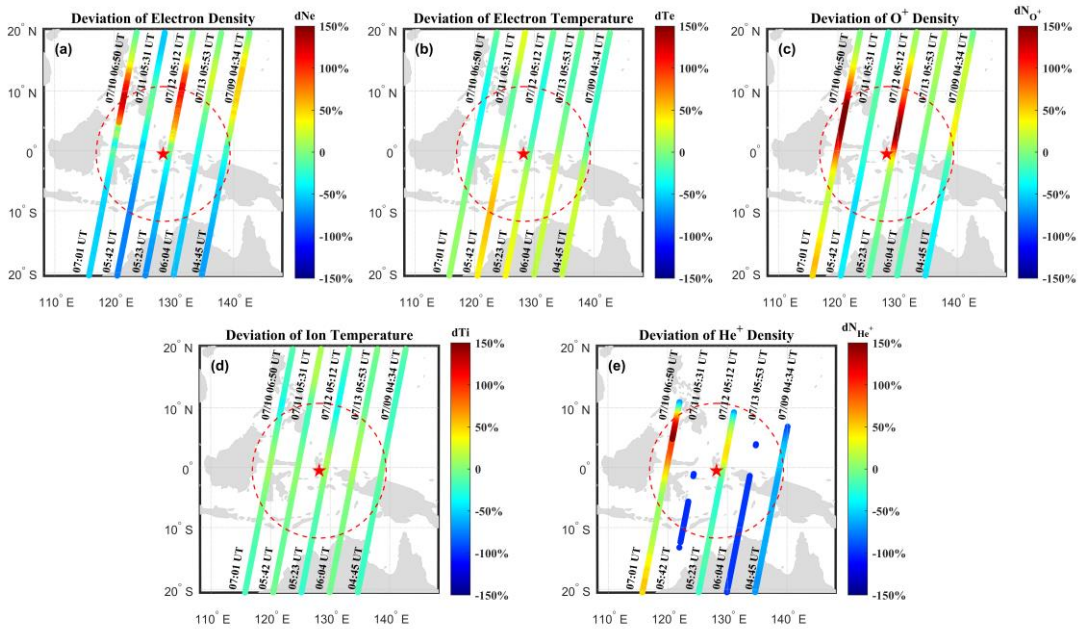

Figure 5. Deviation percentage of plasma parameters from 9 July to 13 July. The red stars represent the epicenter of the earthquake and the red dashed circles represent the preparation zone (ρ =1247.38 km), the precise moments (universal time) of flying above this area are marked at the beginning and end of each orbit.

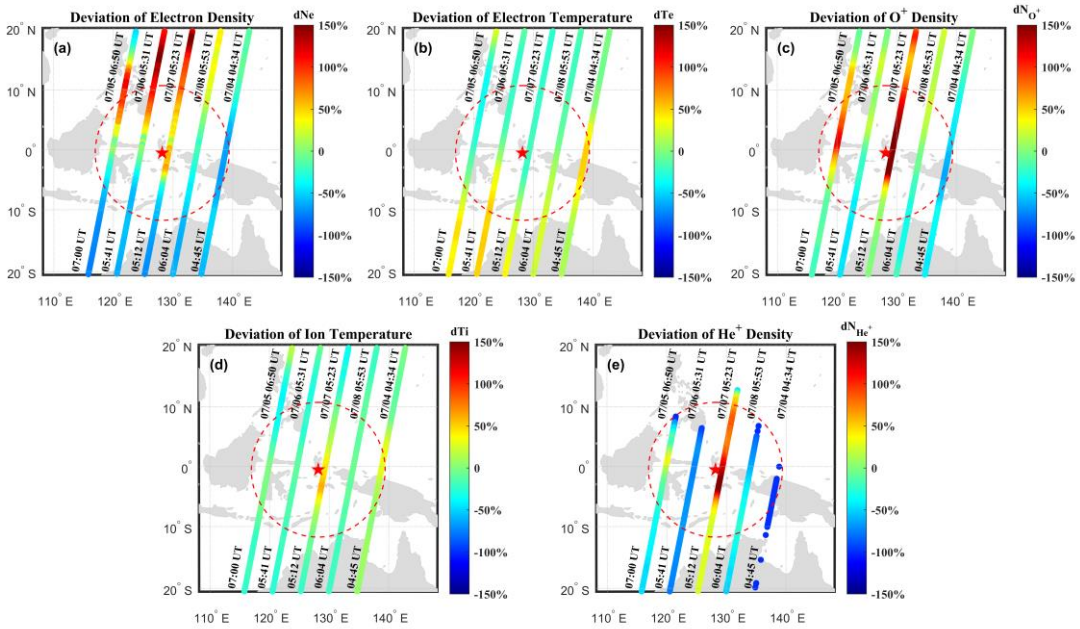

691

692 **Figure 6.** Deviation percentage of plasma parameters from 4 July to 8 July. The red stars
693 represent the epicenter of the earthquake and the red dashed circles represent the
694 preparation zone (ρ =1247.38 km), the precise moments (universal time) of flying above
695 this area are marked at the beginning and end of each orbit.

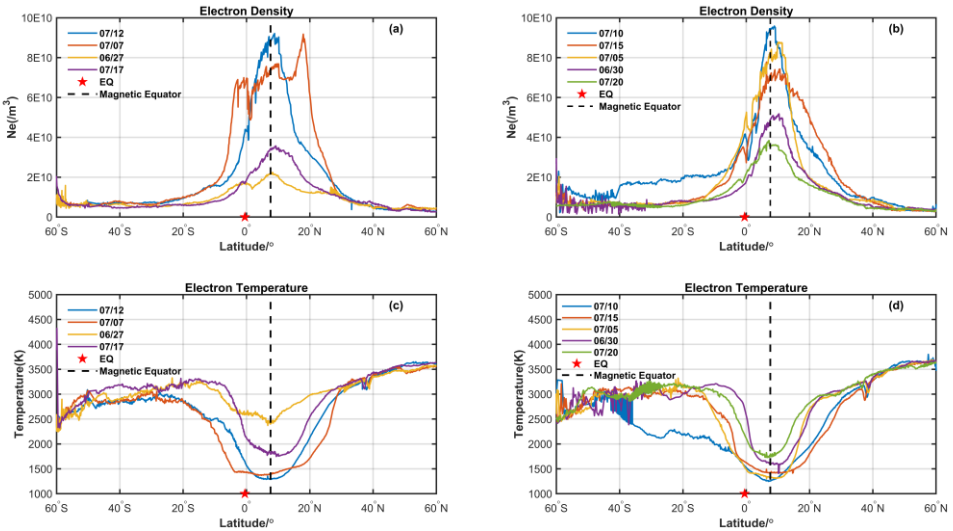

696

697 **Figure 7.** The variations in Ne and Te from the abnormal orbits, and their revisiting orbits
698 along latitude. Red stars represent earthquake epicenters, and the black dotted line in each

699 subfigure represents the magnetic equator.